RESEARCH PAPER

Imprint of paleocurrents, extensional and compressional deformation in the magnetic fabrics of the Permo-Triassic red beds of the Cadí Basin (Eastern Pyrenees)

Ana Simón-Muzás[1] · Ruth Soto[2] · Emilio L. Pueyo[2] · Elisabet Beamud[3] · Belén Oliva-Urcia[1] · Antonio M. Casas-Sainz[1]

Abstract

A magnetic fabric study was carried out in Permo-Triassic continental sedimentary red beds from the Cadí Basin (Eastern Pyrenees). These rocks were deposited on the top of a volcanic sequence when the regional tectonic regime changed from transtension to extension. Standard paleomagnetic cores (cylinders), cubes and irregular fragments were obtained for this study in 25 sites distributed throughout the basin. The "fragment methodology", using oriented irregular fragments in clay-stones, is demonstrated to be successful and replicable. The aims of this study are (i) to interpret the magnetic fabrics in red beds according to sedimentary or tectonic models; (ii) to establish the relationship between the magnetic fabrics in the sedimentary red beds and the magnetic fabrics previously obtained in the underlying volcanic series, and (iii) to compare magnetic fabrics in continental sediments with other basins of the same age to interpret the tectonic scenario in the Iberian plate during Permian and Triassic times. The results obtained reveal a primary magnetic fabric that recorded a syn-sedimentary stretching in two nearly perpendicular directions, WNW-ESE and N-S, linked to basin development. Other sedimentary and tectonic factors, such as paleocurrents and deformation derived from the Alpine compression did not have a significant influence on the development of magnetic fabrics. The geodynamic scenario of the Iberian plate during Late Permian to Triassic times can be explained according to regional trajectories of extensional stress due to the activity of the North-Pyrenean fault zone.

Keywords AMS · Magnetic fabrics · Pyrenees · Permian · Sedimentary rocks · Red beds

Registro de paleocorrientes, deformación extensional y compresiva en las fábricas magnéticas de las facies rojas Permo-Triásicas de la Cuenca del Cadí (Pirineos Orientales)

Resumen

Se ha realizado un estudio de fábricas magnéticas en facies rojas continentales Permo-Triásicas de la Cuenca del Cadí (Pirineos Orientales). Estas rocas se depositaron sobre una secuencia volcánica cuando el régimen tectónico regional cambió de transtensión a extensión. Para este estudio se obtuvieron muestras paleomagnéticas estándar (cilindros), cubos y fragmentos irregulares, en 25 estaciones distribuidas por toda la cuenca. La «metodología de fragmentos», que utiliza fragmentos irregulares orientados en argilitas, ha demostrado ser satisfactoria y reproducible. Los objetivos de este estudio

✉ Ana Simón-Muzás
anasimon@unizar.es

[1] Departamento de Ciencias de La Tierra, Geotransfer-IUCA, Universidad de Zaragoza, 50009 Zaragoza, Spain

[2] IGME, Instituto Geológico y Minero de España, CSIC, Unidad de Zaragoza, 50059 Zaragoza, Spain

[3] Paleomagnetic Laboratory CCiTUB - Geosciences Barcelona (Geo3Bcn), CSIC, 08028 Barcelona, Spain

🄢 Springer

son (i) interpretar las fábricas magnéticas en las capas rojas según modelos sedimentarios o tectónicos; (ii) establecer la relación entre las fábricas magnéticas en las capas rojas sedimentarias y las fábricas magnéticas obtenidas previamente en la serie volcánica subyacente, y (iii) comparar las fábricas magnéticas en sedimentos continentales con otras cuencas de la misma edad para interpretar el contexto tectónico en la placa Ibérica durante los tiempos Pérmico y Triásico. Los resultados obtenidos revelan unas fábricas magnéticas primarias que registraron un estiramiento sinsedimentario en dos direcciones casi perpendiculares, WNW-ESE y N-S, ligado al desarrollo de la cuenca. Otros factores sedimentarios y tectónicos, como las paleocorrientes y la deformación derivada de la compresión alpina, no tuvieron una influencia significativa en el desarrollo de las fábricas magnéticas. El escenario geodinámico de la placa Ibérica durante el Pérmico Tardío al Triásico puede explicarse en función de trayectorias regionales de esfuerzos extensionales debidos a la actividad de la zona de falla Norpirenaica.

Palabras clave AMS · Fábricas magnéticas · Pirineos · Pérmico · Rocas sedimentarias · Facies rojas

1 Introduction

The analysis of anisotropy of magnetic susceptibility (AMS) allows to define the magnetic fabric of rocks and sediments, which is related to the preferred orientation of grains and minerals. AMS is a fast, non-destructive and statistically representative technique that is often superior to visible markers that are scarce at the outcrop level in ancient volcanic and sedimentary rocks.

Magnetic fabrics result from the spatial variation of the magnetic susceptibility (K for normalized volume). The magnetic susceptibility of a rock or sediment is a tensorial property that can be expressed geometrically by a three axes ellipsoid. The orientation and size of the magnetic susceptibility ellipsoid depend mostly on the orientation and magnetic (mainly ferromagnetic s.l. when it is present and paramagnetic) behavior of the minerals within the studied rocks. For this reason, AMS allows us to define the magnetic fabric that can be primary if it shows the original orientation of the minerals during their deposition, or secondary, if minerals were subsequently reoriented by tectonic deformation.

Sedimentary rocks, and in particular continental sediments, such as siltstones and claystones, were the starting point for the development of AMS from its beginning (Graham, 1954) and its application was later extended to igneous rocks, either intrusive or extrusive (Khan, 1962; Knight & Walker, 1988). Some of the most common minerals in sedimentary rocks are phyllosilicates, that in a non-hydrodynamically energetic environment are expected to be oriented with their largest surface parallel to the ground due to their platy shape. In this case, the magnetic fabric is an oblate susceptibility ellipsoid where the minimum susceptibility axis (K_3) is vertical, thus defining a typical sedimentary fabric. This AMS dependence on the shape anisotropy of platy minerals is well known (Kodama & Sun, 1992; Martín-Hernández and Hirt, 2003) and in general, phyllosilicates are the main carriers of susceptibility in sedimentary rocks. However, the presence in much less quantities of iron oxides (ferromagnetic s.l.) can superimpose on the

other magnetic behaviors present in a mineral assemblage (Oliva-Urcia et al., 2009) and dominate the bulk magnetic fabric. The magnetic fabric can be thought of as the sum of the contributions of the different components, showing different magnetic behaviors of the rock.

The interest of magnetic fabrics studies in fine grained continental sediments lies in its extreme sensitivity to very weak deformation episodes which may not produce macroscopic structural markers such as well-defined foliations and lineations (Gracia-Puzo et al., 2021; Parés, 2015). The changes in the shape and orientation of magnetic susceptibility ellipsoids due to a progressive increase in strain has been extensively described in mudrocks in compressional settings (Parés et al., 1999): in the early stages of deformation, the magnetic fabric shows K_3 axes perpendicular to bedding and a cluster of K_1 axes perpendicular to the direction of compression/shortening (see also Larrasoaña et al., 2004; Soto et al., 2009). Regarding medium-coarse-grained sediments such as sandstones that were deposited in an hydrodynamically energetic environment to a greater or lesser degree, the preferred mineral orientation and therefore magnetic fabrics orientation are conditioned by currents (Pueyo-Anchuela et al., 2010; Felleti et al., 2016; Stachowska et al., 2020). In this context, mineral grains are oriented with their long axis parallel to the current and magnetic fabrics present their K_1 axes also parallel to it (Piper, 1996). However, there are cases where K_1 axes are perpendicular to the current direction when mineral grains have been transported by rolling in ripples (Piper, 1996). For that reason, the study of magnetic fabrics in sedimentary rocks must be addressed considering all these factors that influence their final shape and orientation.

The Pyrenees have attracted numerous AMS studies in Mesozoic and Cenozoic sedimentary rocks, especially in their Central and Western sectors (e.g. Pocoví et al., 2014 and references therein). However, the eastern sector of the Pyrenees shows a lower amount of this kind of data, except for the abundant studies of Carboniferous granites (Porquet et al., 2017 and references therein) and analysis of

deformation linked to cleavage development (Parés et al., 1999).

The Upper Carboniferous-Permian rocks of the Cadí Basin (Eastern Pyrenees) are volcanic and volcaniclastic in the lower part of the stratigraphic succession, and sedimentary, with a clear continental imprint, in its upper part. The present work aims to exploring the limits of the application of AMS in rocks that i) present a high degree of chemical alteration (see Gisbert, 1981; Bixel, 1984), ii) show a varied range of lithologies, from fine-grained sandstones (in which the influence of paleocurrents can be present) to siltstones and claystones and iii) have been affected by, firstly, extensional or transtensional tectonics and, subsequently, by compressional tectonics. The objectives are i) to recognize the dominant magnetic fabrics pattern in the above-mentioned lithologies; ii) to characterize the carriers of the magnetic susceptibility and iii) to establish the relationship between magnetic fabrics in volcanic and volcaniclastic rocks with those obtained in continental sediments deposited in the same basin (the Cadí Basin) under a (presumably) similar tectonic regime. Red beds were deposited in different environments with different energy (fluvial to lacustrine) and were sampled with the aim to determine if the magnetic fabrics were acquired primarily (during the deposit), responding or not to the action of hydrodynamic flows (paleocurrents), or secondary, that is, related to the prevailing tectonic regime. Additionally, these sedimentary units were deposited in an intramountainous basin that since their origin underwent different tectonic scenarios due to their evolution as a part of the Variscan orogen (undergoing a Late-Variscan fracturing and volcanic stage) and subsequently as a part of the Pyrenean belt.

The results obtained here are the complement of the detailed magnetic fabric study performed in volcanic and volcaniclastic rocks (Simón-Muzás et al., 2022) in the lower part of the stratigraphic succession (Grey Unit and Transition Unit, GU and TU of Gisbert, 1981). In that study, the origin of the magnetic fabrics was interpreted as primary and allowed us to establish a NW–SE direction (without establishing the sense of the flow) for the paleocurrents of magma, ignimbrites and other volcaniclastic products. The deposition of volcanic rocks, and hence the magnetic fabrics distribution was also closely controlled by the fault pattern developed during Late Carboniferous-Permian times.

2 Geological context and stratigraphy

The Cadí Basin is located in the Eastern Pyrenees (Fig. 1A) and is one of the Late Carboniferous-Permian basins that are distributed along a discontinuous WNW-ESE band in the southern edge of the Axial Zone (Gisbert et al., 2024). These basins have undergone changing tectonic regimes since their formation. They were originated at Late Carboniferous-Early Permian times during the dismantling of the Variscan orogen. At this stage, volcanic episodes linked to crustal- or lithosphere-scale faults occurred in a tectonic context that changed from extension to transtension (Gretter et al., 2015). During that period, the basins were filled with fluvio-lacustrine sediments and volcanic products. Subsequently, they evolved during the two rift-postrift Late Palaeozoic-Mesozoic cycles that also affected the Variscan rocks (e.g. Barnolas & Pujalte, 2004; Muñoz, 2019). During the Late Cretaceous to Miocene, these basins were affected by the Alpine orogeny due to the convergence between the European and Iberian plates (e.g. Muñoz, 1992). The Cadí Basin was particularly affected by the Pyrenean compression between the Early Eocene and the Late Oligocene (Vergés et al., 2002), when it was incorporated into the Orri thrust unit (Muñoz, 1992; Saura & Teixell, 2006) and all the stratigraphic succession filling the ancient basin was tilted towards the south.

The Orri thrust unit presents an anticline geometry elongated in an E-W direction. It is constituted by sandstones, shales and siltstones with an attributed Cambro-Ordovician age (Hartevelt, 1970). Unconformably overlying this unit, there are Upper Ordovician conglomerates, Silurian shales and Devonian limestones. This set of rocks constitutes the Variscan basement, that is overlain by the Late Carboniferous-Permian rocks. The Orri unit is topped by the Rialp thrust sheet and underlain by the Erta and Nogueres thrust units, all of them forming the Axial Zone antiformal stack (Muñoz, 1992). The main transport direction of these thrusts is SSW (Saura & Teixell, 2006).

Sedimentary and volcanic rocks from the Cadí Basin were described in detail by Gisbert (1981), who defined four lithostratigraphic units based on paleoclimatic conditions existing during their sedimentation (Fig. 1B, C). This nomenclature its widely used for the Carboniferous-Permian rocks of these intramountainous basins. The Grey Unit (GU) is the basal unit; it lies unconformably onto the pre-Variscan basement, and is composed by detrital, volcanic and volcaniclastic deposits. The Transition Unit (TU) appears discontinuously in the area and is composed mainly by detrital sediments within which volcanic and volcaniclastic deposits are occasionally intercalated. The Lower Red Unit (LRU) is formed by claystones, sandstones and microconglomerates with interspersed volcanic rocks. The volume of volcanic products decreases towards the top of the unit. In the Upper Red Unit (URU), detrital rocks are also dominant and only occasionally volcanic rocks are described.
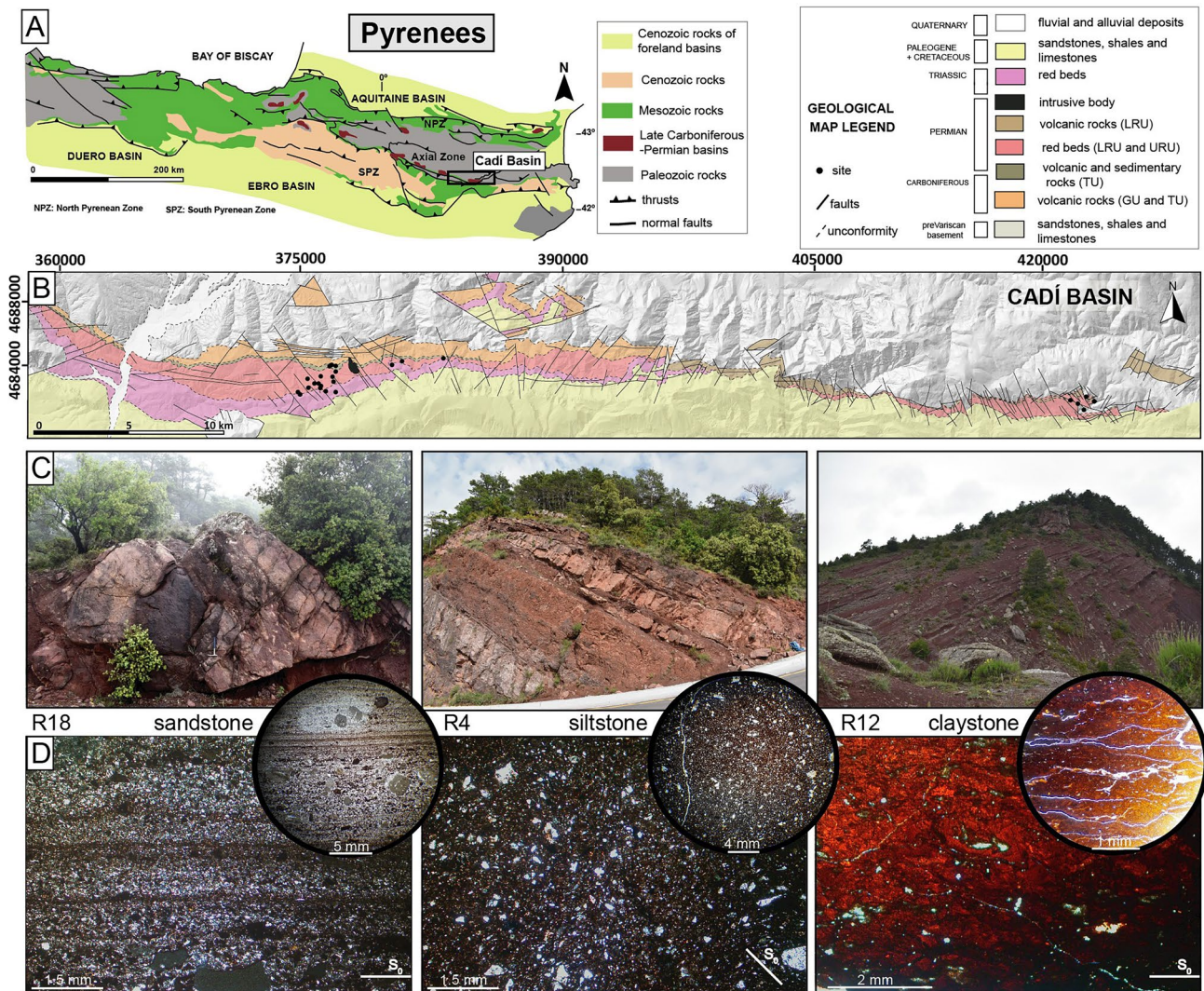
Fig.1 **A** Geological map of the Pyrenees and situation of the Carboniferous-Permian basins; the Cadí Basin squared in black; **B** Geological map digitized from Gisbert (1981). Black circles sampling sites; **C** Different views of the red bed outcrops sampled in the present study; **D** Three thin sections in parallel polarizers for the three sampled lithologies. The bedding plane is marked with a white line (S_0)

3 Methodology

3.1 Sampling campaign and field work

A total of 25 sites were sampled for the AMS study in red bed outcrops of the TU, LRU, URU (Permian) and the Triassic. The sampling lithologies (Fig. 1D) were claystones (six sites), siltstones (seven sites) and medium/coarse-grained sandstones (12 sites). Conglomerates and coarse-grained sandstones were excluded from sampling.

Samples were obtained in the field with an electrical drill in siltstones and with a gas-powered drill in sandstones, both water-cooled, to obtain oriented cores. Oriented blocks were taken (two or three oriented blocks per site) in six sampling sites (R5, R8, R13st, R20, R21 and R22) where the access

to the outcrop with the drills was difficult. In the claystone sites (six sites, Table 1), oriented fragments of small size and irregular shapes were extracted manually due to their brittle nature (see in Table 1 sample type for each site). All samples were oriented with a magnetic compass and sampling sites were positioned with a GPS. Oriented samples were cut using a radial saw (non-magnetic steel) in the laboratory: cores to 2.1 cm height and 2.5 cm-diameter standard cylinders and blocks to 2.1 cm-edge cubes. Ten standard cylinders were obtained, on average, in each drilled sampling site, and nine to 24 standard cubes were obtained from oriented blocks. The oriented small irregular fragments from claystone sites were placed inside a methacrylate cube with 2 cm edge with its oriented face parallel to one side of the cube. They were then properly fixed in with absorbent cotton, a

Table 1 Magnetic susceptibility ellipsoid data. Name of the site, coordinates (UTM), Sample type: cyl for cylinder, cube for cube and frag for irregular fragments

Site	Sample type	X UTM 31 EPGS:25,831	Y UTM 31 EPGS:25,831	N	Lit	Kmean (·10^-6)	std.dev (·10^-6)	K₁ (in situ)	conf. ang	K₃ (in situ)	conf. ang	K₁ (corrected)	conf. ang	K₃ (corrected)	conf. ang	Pj	e	T	e	S0 (D.D)
R1sd	cyl	376,345.99	4,684,228.66	10	sd	271.6	94.65	135.8/31.2	33.6/10.2	39.9/9.7	48.2/7.7	324.7/47.3	33.6/10.3	60.1/47.3	48.2/7.7	1.019	0.004	0.221	0.225	186/50
R1st	cyl	376,340.83	4,684,230.42	7	st	355.8	135.2	84.0/21.3	37.0/10.4	339.6/32.5	22.1/12.0	105.6/22.4	37.0/10.4	287.2/67.6	22.1/12.0	1.019	0.005	0.027	0.316	186/50
R2st	cyl	376,353.297	4,684,131.492	5	st	225.8	134.9	90.3/14.3	12.6/2.0	301.2/73.5	10.4/1.3	270.4/9.6	12.6/2.0	56.3/78.4	10.4/1.3	1.037	0.011	0.236	0.28	095/24
R2sh	frag	376,346.564	4,684,136.469	12	cl	347.4	45.6	75.0/2.4	51.7/14.5	331.1/79.6	17.3/16.9	76.9/6.4	51.7/14.5	190.1/74.1	17.3/16.9	1.034	0.012	0.4	0.354	175/25
R3	cyl	376,436.149	4,684,044.640	8	st	268.3	49.99	348.2/6.1	42.0/10.3	210.9/81.7	40.3/24.9	352.9/13.2	42.0/10.3	112.5/64.6	40.3/24.9	1.024	0.009	0.454	0.214	095/28
R4	cyl	376,419.14	4,683,686.11	8	st	392.3	86.07	22.0/22.3	13.5/12.7	161.2/61.5	12.8/6.2	22.0/22.3	13.5/12.7	161.2/61.5	12.8/6.2	1.011	0.001	0.248	0.378	170/41
R5	cube	376,484.63	4,683,533.12	19	st	107.4	42.04	135.4/7.5	28.6/19.1	40.8/30.9	36.1/15.1	315.0/24.4	28.6/19.1	60.2/30.0	36.1/15.0	1.031	0.018	0.297	0.424	139/32
R6	frag	376,340.546	4,683,248.655	11	cl	301.9	43.5	79.4/9.5	28.4/11.0	328.2/65.1	12.0/6.3	85.6/13.5	28.4/11.0	237.1/74.7	12.0/6.2	1.027	0.019	0.422	0.247	180/30
R7	cyl	375,582.04	4,683,089.22	11	sd	184.4	41.91	222.4/26.1	24.5/6.9	355.8/54.5	8.4/6.0	37.9/2.5	24.4/6.9	276.7/85.2	8.5/6.0	1.023	0.013	0.338	0.344	184/35
R8	cube	375,626.599	4,683,041.511	11	st	114.3	24.46	214.7/10.7	39.4/4.9	340.2/72.0	13.9/4.7	208.7/18.1	39.3/4.9	55.9/69.9	13.9/4.7	1.057	0.012	0.566	0.476	104/24
R9	cyl	375,971.407	4,682,937.678	9	sd	181.6	31	095.0/11.2	25.7/12.2	348.7/54.7	16.1/11.8	277.0/4.0	25.7/12.2	58.6/84.9	16.1/11.9	1.028	0.003	0.323	0.299	160/34
R10	frag	375,826.674	4,682,762.542	9	cl	201.9	21.7	136.2/15.8	18.1/3.4	19.8/57.6	24.8/4.6	317.6/3.6	18.1/3.4	59.8/73.5	24.8/4.6	1.047	0.036	0.328	0.383	170/23
R11	cyl	376,134.789	4,682,685.166	9	sd	178.9	20.17	102.6/21.6	14.4/5.0	322.4/62.7	9.5/6.3	108.5/21.2	14.5/5.0	291.1/68.8	9.5/6.4	1.015	0.005	0.186	0.303	194/15
R12	frag	375,462.436	4,682,555.744	16	cl	335.4	10.6	139.7/18.6	27.6/7.0	337.3/70.5	12.1/5.8	319.1/76.4	27.7/7.0	96.0/81.2	12.1/5.8	1.071	0.008	0.573	0.081	139/25
R13st	cube	374,933.038	4,682,293.344	9	st	119.8	32.46	98.2/18.3	34.3/1.7	299.5/70.4	24.2/6.8	280.4/6.5	34.3/1.7	164.9/75.1	24.2/6.8	1.085	0.025	0.779	0.112	139/32
R13sh	frag	374,932.864	4,682,297.421	10	cl	214	23.6	101.2/11	20.4/6.6	345.2/66.1	6.8/5.0	103.7/2.1	20.4/6.6	282.8/87.9	6.8/5.0	1.074	0.036	0.523	0.331	170/23
R14	frag	376,537.455	4,682,383.731	14	cl	281.8	16.1	335.6/10.8	53.1/13.7	193.8/76.4	17.2/13.5	335.6/10.8	53.1/13.7	193.8/76.4	17.2/13.5	1.058	0.011	0.685	0.214	180/30
R15	cyl	379,707.948	4,684,664.751	12	sd	380	84.11	95.4/15.3	7.4/3.7	333.3/62.7	18.9/5.0	104.2/10.8	7.4/3.7	229.4/71.7	18.9/5.0	1.029	0.007	-0.228	0.202	183/37
R16	cyl	380,298.675	4,684,420.480	11	sd	229.3	77.67	174.8/34.9	18.3/8.8	355.9/55.1	11.1/5.1	176.9/8.4	18.3/8.8	326.3/80.3	11.1/5.1	1.03	0.019	0.16	0.427	187/27
R17	cyl	382,882.432	4,684,737.269	10	sd	313.5	87.64	275.0/24.4	9.4/3.0	29.8/42.8	11.2/7.3	263.9/2.0	9.4/3.0	143.0/86.0	11.2/7.3	1.031	0.011	-0.351	0.212	205/49
R18	cyl	419,106.946	4,681,389.905	24	sd	160.5	42.45	155.5/47.4	7.1/2.6	37.8/23.2	19.1/2.9	351.6/1.1	7.1/2.6	85.1/72.0	19.1/2.9	1.046	0.013	-0.292	0.209	200/58
R19	cyl	419,552.680	4,681,246.213	10	sd	391.8	77.09	161.4/55.2	12.4/5.7	23.9/27.1	7.6/5.5	357.0/5.4	12.5/5.9	131.1/82.2	7.6/5.6	1.013	0.004	-0.028	0.439	196/66
R20	cube	419,661.891	4,681,156.694	9	sd	97.01	4.326	53.5/60.9	3.1/1.7	281.3/20.5	3.3/2.3	143.2/27.7	3.1/1.6	246.2/23.2	3.2/2.4	1.016	0.001	-0.114	0.094	172/74
R21	cube	420,038.533	4,681,704.916	14	sd	446.4	98.46	175.6/33.5	6.9/4.0	59.4/33.8	44.4/3.7	178.9/2.0	6.9/3.9	86.4/52.2	44.3/3.7	1.029	0.006	-0.553	0.206	195/33
R22	cube	420,269.446	4,681,534.203	13	sd	337.7	106.4	250.9/16.9	14.9/6.5	357.4/43.0	50.1/6.5	65.9/7.2	50.1/6.5	194.6/78.6	14.8/5.2	1.017	0.009	-0.063	0.409	181/58

N: number of specimens, Lit: lithology: sd: sandstones, st: siltstones, cl: claystones, Km: magnitude of mean magnetic susceptibility (10^{-6} S.I), K_1 and K_3-mean (trend and plunge) of the magnetic lineation and of the pole to the magnetic foliation (Jelinek, [1977]) in situ and after tectonic correction (corrected). Conf. ang: major and minor semi-axes of the 95% confidence ellipse (Jelinek, [1981]). Pj: corrected anisotropy degree (Jelinek, [1981]); T shape parameter (Jelinek, [1981]); e: standard deviation in situ; S0 (D.D): bedding plane dip direction

material that shows a dominant weak diamagnetic behavior that does not affect the rock magnetic susceptibility signal (Fig. 2).

Structural data (bedding planes, fractures, faults and striae) were collected from 17 sites along a N-S section in El Ges zone (central zone) where most of the sites are located. Additionally, measurements of scours and gutters were taken to obtain paleocurrent directions in a base of a conglomerate bed located at the top of the URU. One site (R12) was sampled in the underlying claystones. The purpose of this data collection is to compare the AMS results with the structural data and paleocurrents directions and to recognize the influence of tectonic stresses and hydrodynamic flows in the final shape and orientation of the magnetic fabrics. Structural data and paleocurrents were represented in lower-hemisphere, equal-area stereoplots (Allmendinger et al., 2012).

3.2 AMS analysis

The study of anisotropy of magnetic susceptibility is based on the determination of the directional variation of the susceptibility (K) by applying a low intensity magnetic field (300 A/m) in different orientations to a standard specimen (cylinder or cube). The magnetic susceptibility (K) of a rock depends on the orientation of its mineral particles and is conditioned by their magnetic behaviors: ferromagnetism, paramagnetism and diamagnetism. Magnetic susceptibility is a dimensionless property in the International System (SI) that can be expressed mathematically as a second order tensor or geometrically as an ellipsoid where its three principal orthogonal axes are $K_1 > K_2 > K_3$. The magnetic susceptibility ellipsoid was described by Nye (1957) and the parameters used for its characterization (Jelinek, 1981) are: (a) mean susceptibility (Km or Kmean) expressed as $Km = (K_1 + K_2 + K_3)/3$, (b) corrected degree of anisotropy (Pj) expressed as $Pj = \exp\sqrt{2((n_1-n)^2 + (n_2-n)^2 + (n_3-n)^2)}$ and (c) shape parameter (T) expressed as $T = (2n_2-n_1-n_3)/(n_1-n_3)$ where n_1, n_2, n_3 are the natural logarithms of K_1, K_2 and K_3.

A correction to the mean magnetic susceptibility was applied in the case of irregular fragments (different volume and mass, non-standard specimens) of claystone sites (see Supplementary material). The mass of each fragment was measured, and a mean density value was also calculated according to Archimedes' principle, $\rho = $ dry weight/ (dry weight-weight immersed in water) in cgs units. The methacrylate cubes containing the fragments were measured in 15 manual routine positions.

The AMS measurements at room temperature (RT-AMS) were performed in the Magnetic Fabrics Laboratory of the Zaragoza University (Spain), using a KLY-3S Kappabridge (AGICO Inc, Czech Republic) and SUSAR software (AGICO Inc, Czech Republic). The Anisoft 5.1.03 software (Chadima and Jelinek, 2019) was used for data processing. A total of 285 oriented specimens in the sedimentary red beds were analyzed.

In order to check the origin of the magnetic fabrics three thin sections perpendicular to the bedding plane were carried

Fig. 2 **A** Oriented standard specimen types analyzed in the present study: cylinders, irregular fragments, and cubes. **B** Oriented block sample from which the oriented irregular fragments have been obtained in site R12. **C** Oriented irregular fragments specimens from site R12. D) KLY-3 Kappabridge (AGICO Inc, Czech Republic) used for the analysis of the magnetic fabrics
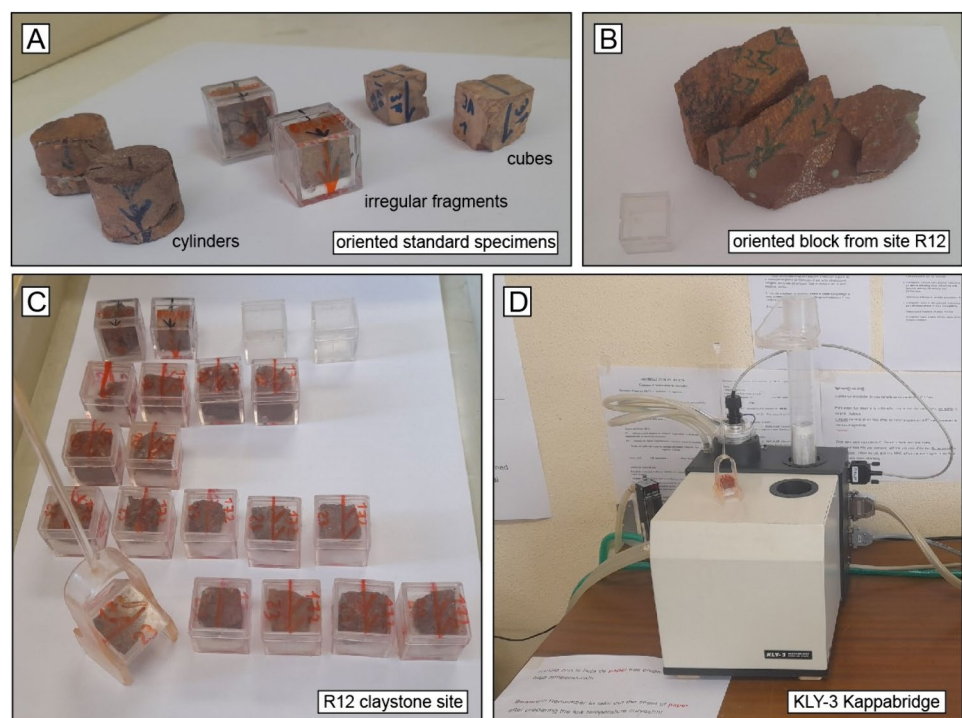
out in three different lithologies (R18 sandstone, R4 siltstone and R12 claystone site).

3.3 Rock magnetism

Measurements of AMS were complemented with nine temperature-dependent susceptibility curves to elucidate the magnetic carriers in the studied rocks. The presence of paramagnetic minerals is determined from the hyperbolic geometry of the temperature-dependent susceptibility curves. Paramagnetic minerals show a dependence of susceptibility on temperature defined by the Curie–Weiss law: $Kp = C/(T - \theta)$, where Kp is the paramagnetic fraction of the total magnetic susceptibility, C is the Curie constant of the mineral, T is the absolute temperature in Kelvin and θ is the paramagnetic Curie temperature. On the other hand, ferromagnetic minerals identification depends on their Curie (T_C) or Néel (T_N) temperature. The analyses were performed in the KLY-3S Kappabridge with a coupled CS-3 furnace and they encompassed a temperature range between 40 to 700ºC in argon atmosphere in order to avoid mineral oxidations during heating. These samples were powdered in an agate mortar (0.1–0.3 g per sample). Sample processing was carried out with SUSTE software (AGICO Inc., Czech Republic) and a correction of the free furnace (measure of the CS3 without the sample) and a normalization of the susceptibility values to a standard-volume specimen were applied in each analyzed curve. Results were interpreted with the Cureval 8 software (Chadima & Hrouda, 2012). Thermal demagnetization of the isothermal remanent magnetization (IRM) is also available from a previous paleomagnetic study (Simón-Muzás et al., 2023).

The hysteresis loops and the temperature-dependent induced magnetization curves (sites R1st, R6, and R9) were performed in a MPMS3 Quantum Design Squid with a SQUID sensor magnetometer system at the University of Zaragoza (Spain). The hysteresis loops were performed at room temperature applying a progressively higher induced magnetic field up to 4 T and subsequently decreasing it in the opposite direction. In the temperature-dependent induced magnetization curves, the analyzed sample is cooled down to 5 K and then a 3 T field is applied; then the sample reaches room temperature (300 K) and a magnetic field of 3 T is applied again; finally, it is cooled down to 5 K. The measurements were taken during the heating and the second cooling path.

4 Results

4.1 Magnetic fabrics: RT-AMS

The mean value of K_m at site level is 256.58·10^{-6} SI, and it ranges between 97.01 in site R20 to 446.40·10^{-6} SI in site

R21 (Table 1; Fig. 3A, B). A relationship between K_m and the lithological type of the studied sites is ruled out. Regarding the magnetic ellipsoids characterization (Table 1), the Pj parameter ranges between 1.011 and 1.085 at site level (sites R4 and R13sh) and shows no correlation with K_m values. The T parameter does not show a correlation with K_m and ranges between -0.553 and 0.779 (sites R21 and R13sh). If we consider the lithology, siltstones and claystones only show oblate magnetic ellipsoids whereas sandstones are the only lithology that presents prolate magnetic ellipsoids in seven sites (see T parameter in Table 1). A positive correlation between the Pj and T parameters is observed only in siltstones (Fig. 3C).
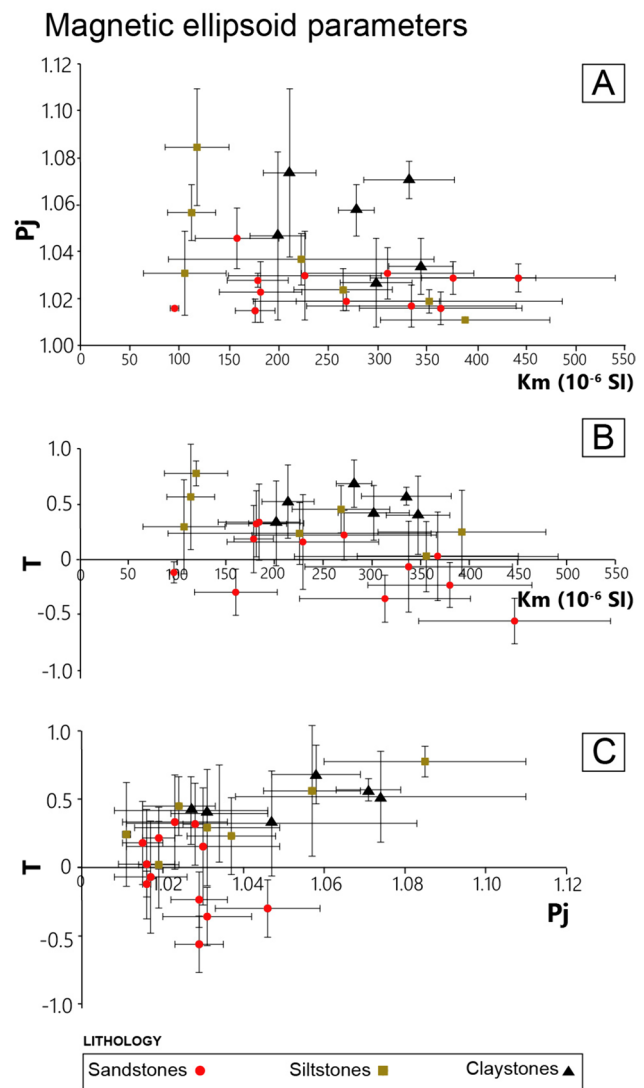

Fig. 3 Diagrams of the magnetic ellipsoid parameters depending on lithological types: **A** Corrected anisotropy degree (Pj) versus bulk magnetic susceptibility (Km). **B** Shape parameter (T) versus bulk magnetic susceptibility (Km). **C** Shape parameter (T) versus corrected anisotropy degree (Pj). Averaged values from each sampled site and standard error

Concerning the orientation of the magnetic fabrics, K_3 is arranged perpendicular to the bedding plane in average or distributed within a girdle with the K_2 axes (sites R1st, R18 and R21) also perpendicular to it. Only site R20 does not show this relationship between the minimum magnetic axis and the bedding plane (Fig. 4). After tectonic correction, the K_3 axes become vertical or subvertical except at sites where it is distributed in a girdle with K_2 or in site R20 (Fig. 5). The α_{95} confidence angle (Table 1) is not higher in claystones sampled using small oriented fragments, which allows us to discard that the sampling methodology (irregular fragments with small orientation surface) and analysis (15 manual positions) could have introduced some additional uncertainty or bias.

In general, the orientation of K_1 axes before or after the tectonic correction shows either an E-W direction (sites R1sh, R2sh, R2st, R6, R9, R11, R13sh, R13st, R15, and R17) or a N-S direction (sites R3, R4, R14, R16, R18, R19, R21 and R22); both of them well clustered. Intermediate directions are found in the rest of sites, either NW–SE (sites R1st, R5, R10, R12 and R20) or, more rarely, NE-SW (sites R7 and R8). All these directional maxima revealed in individual sites can also be observed in the stereoplot summarizing the whole dataset (Fig. 7A). If we consider the whole dataset, an overall pattern showing a dominant N-S and an WNW-ESE direction for K_1 can be defined after tectonic correction. Both K_1 and K_3 axes show a better grouping after tectonic correction pointing to an early acquisition of magnetic fabrics in the studied rocks prior to any subsequent tectonic event.

4.2 Rock magnetism characterization

Sites R4, R9, R12 and R15 show reversible temperature-dependent magnetic susceptibility curves (heating and cooling paths are superimposed or close) and sites R1st, R2st, R6, R10 and R21 are clearly irreversible, a fact that is not linked with the grain size or the lithology (claystones, siltstones or sandstones). Magnetic mineralogy consists of a mixture of paramagnetic and ferromagnetic phases (Fig. 6). The paramagnetic behavior can be inferred from the concave-hyperbolic shape at the beginning of the heating curves (Curie–Weiss law, e.g. Parés & Van der Pluijm, 2002) in sites R2st, R4, R9 and R15. Ferromagnetic minerals are inferred from the decay at 580ºC and the decay at 670ºC in the heating curves that correspond to the Curie temperature (T_c) of magnetite and hematite respectively. An abrupt decay at 120ºC is only observed in site R21. Cooling paths show higher susceptibilities than heating paths; their traces diverge steeply at 580ºC pointing towards the neoformation of a mineral with this T_c during heating.

The temperature-dependent induced magnetization curves present the decays around 580ºC pointing towards the presence of magnetite. The hysteresis loops do not show a wasp waist, corroborating the presence of a single ferromagnetic fraction of magnetite in the three analyzed sites (R1st, R6 and R9). The two branches of the hysteresis loops describe a straight line with a positive slope due to the presence of paramagnetic minerals (Fig. 6).

4.3 Paleocurrents and structural data

The scours and gutters measured in the base of a conglomerate bed (Fig. 7A, C) located at the top of the URU indicates, in terms of paleocurrents, an WNW-ESE flow direction, that is very similar to the flow direction obtained in the volcaniclastic rocks deposited during the Late Carboniferous (Simón-Muzás et al., 2022).

The tectonic structures are mainly faults and fractures. Faults (Fig. 7A, E) show slickenside striations and often a mineralized film of quartz or calcite. Shear criteria include crystal growth and R (Riedel, 1993) fractures associated with shear along the main fault plane. Most faults are normal after restoring the beds to the horizontal and many of them are arranged in conjugate systems. Their syn-sedimentary origin can be often assessed by the different thickness of strata in their hanging wall and foot wall. Reactivations of normal faults as reverse faults can also be observed. The fault planes display two main directions: a subvertical N–S-set and a WNW–ESE-set dipping 55º towards the south. After tectonic correction they are arranged in N–S and E–W directions. Interestingly, slickenside striations indicate a transtensional component for the E–W fault set and reactivation, under a strike-slip regime, for the N-S set.

Fractures without observable movement between their two blocks have also been observed (Fig. 7A, B and D). Most of them are perpendicular to the bedding and display two directional maxima: N100E oriented poles (after restoring the bedding to the horizontal) and N-S oriented poles (this maximum can be divided into two, NNE–SSW and NNW–SSE). The main set of fracture planes shows a NNW–SSE direction.

4.4 Comparison between magnetic fabrics and structural data

Comparing AMS results with the structural data and paleocurrents directions allows us to recognize and discuss the role of tectonic stresses and hydrodynamic flows in the final shape and orientation of the magnetic fabrics.

Large-scale faults of the Cadí Basin (Fig. 8) show at present two main directions: NNW-SSE and E-W. The orientation of the magnetic lineation (K_1 mean axis) (Fig. 8) is oblique (R1sd, R1sh, R2sh, R2st, R4, R6, R7, R8, R9, R11, R13sh, R13st, R14, R15, R16, R17, R18, R19, R21, R22) or parallel (sites R3, R5, R10, R12 and R20) to the strike of the
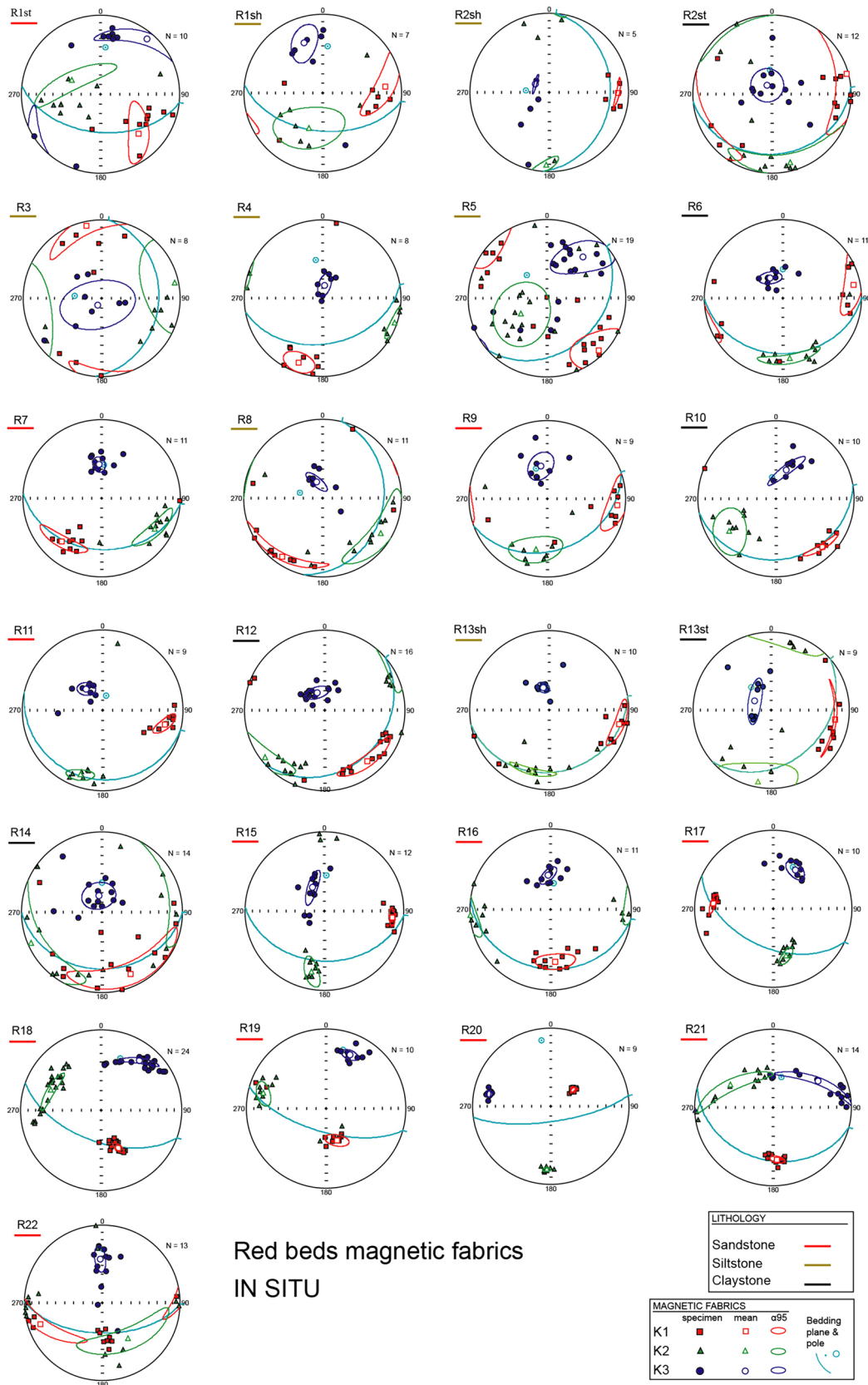
Fig. 4 AMS ellipsoids obtained for each sampling site with 95% confidence ellipses (Jelinek, 1977). The projection of the bedding plane and its pole is represented. Before tectonic correction
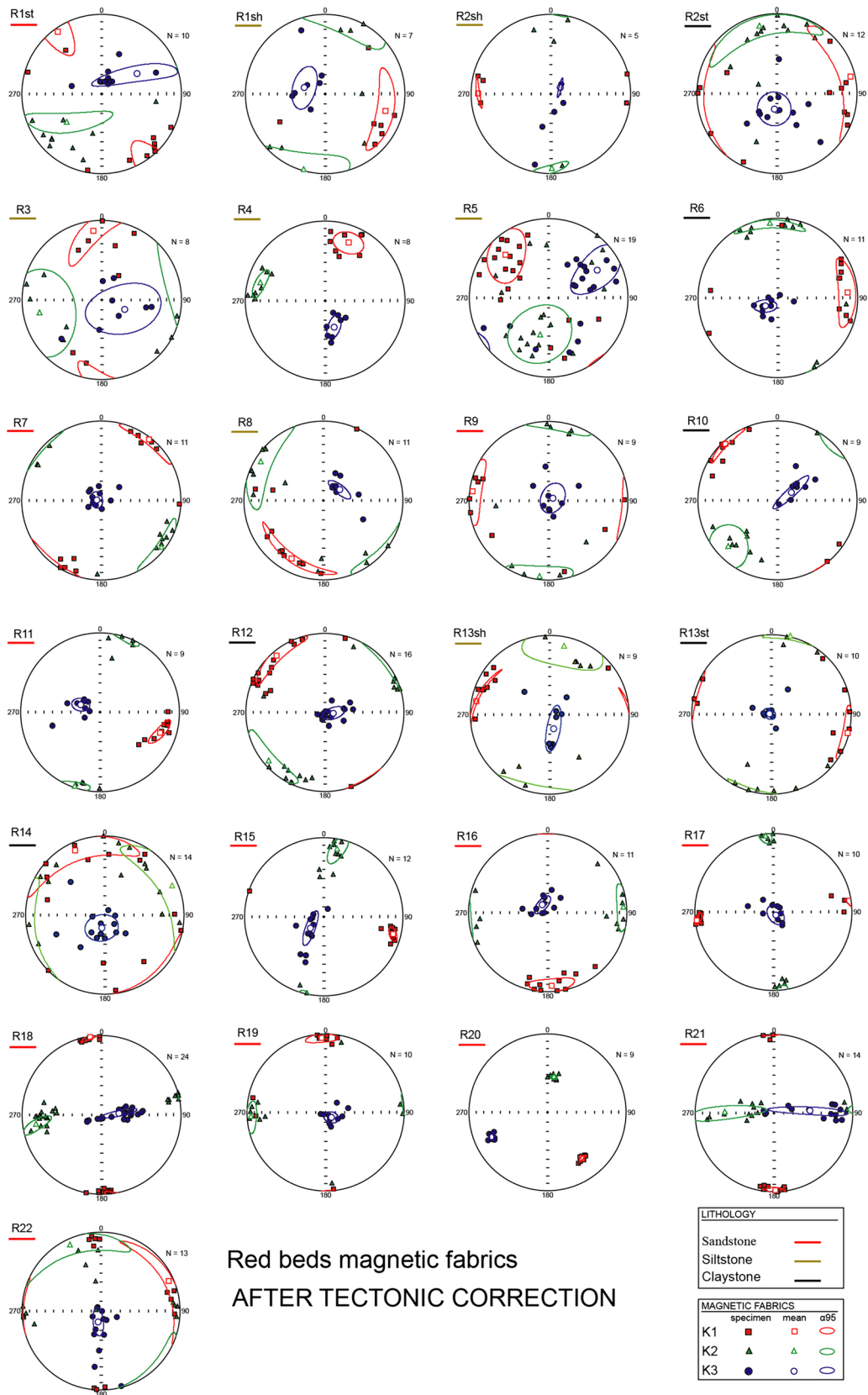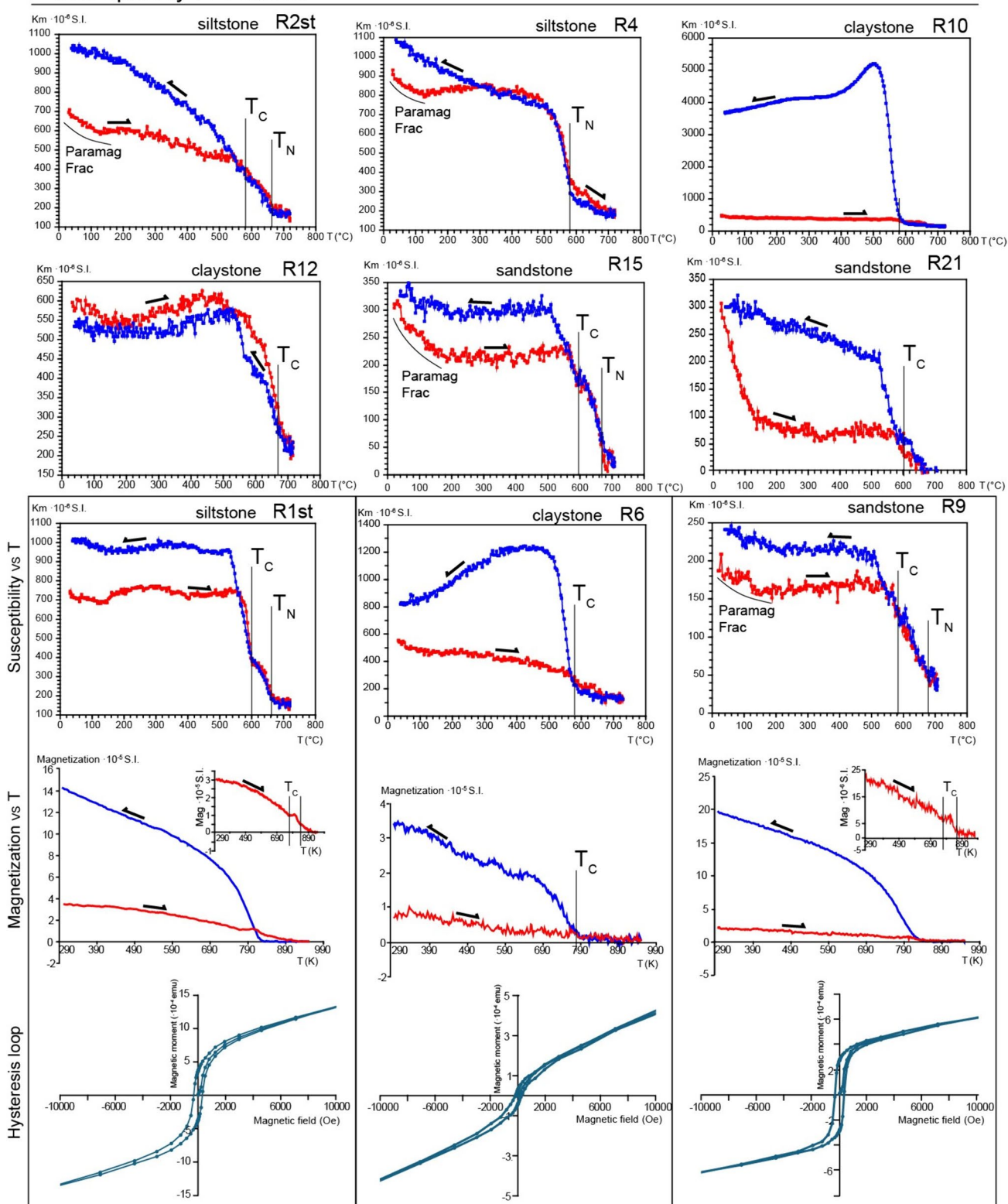
Fig. 5 AMS ellipsoids obtained for each sampling site with 95% confidence ellipses (Jelinek, 1977). The projection of the bedding plane and its pole is represented. After tectonic correction

Fig. 6 Temperature-dependent susceptibility curves (40 to 70ºC) of heating (in red) and cooling (in blue) for the eight analyzed curves, where i) the non-reversibility curves, ii) the concave-hyperbolic shape indicative of paramagnetic minerals and iii) the Curie temperature of the ferromagnetic s.l. mineral can be observed. Below, magnetization-temperature curves and hysteresis loops of three selected sites (R1st: siltstone, R6: claystone and R9: sandstone)
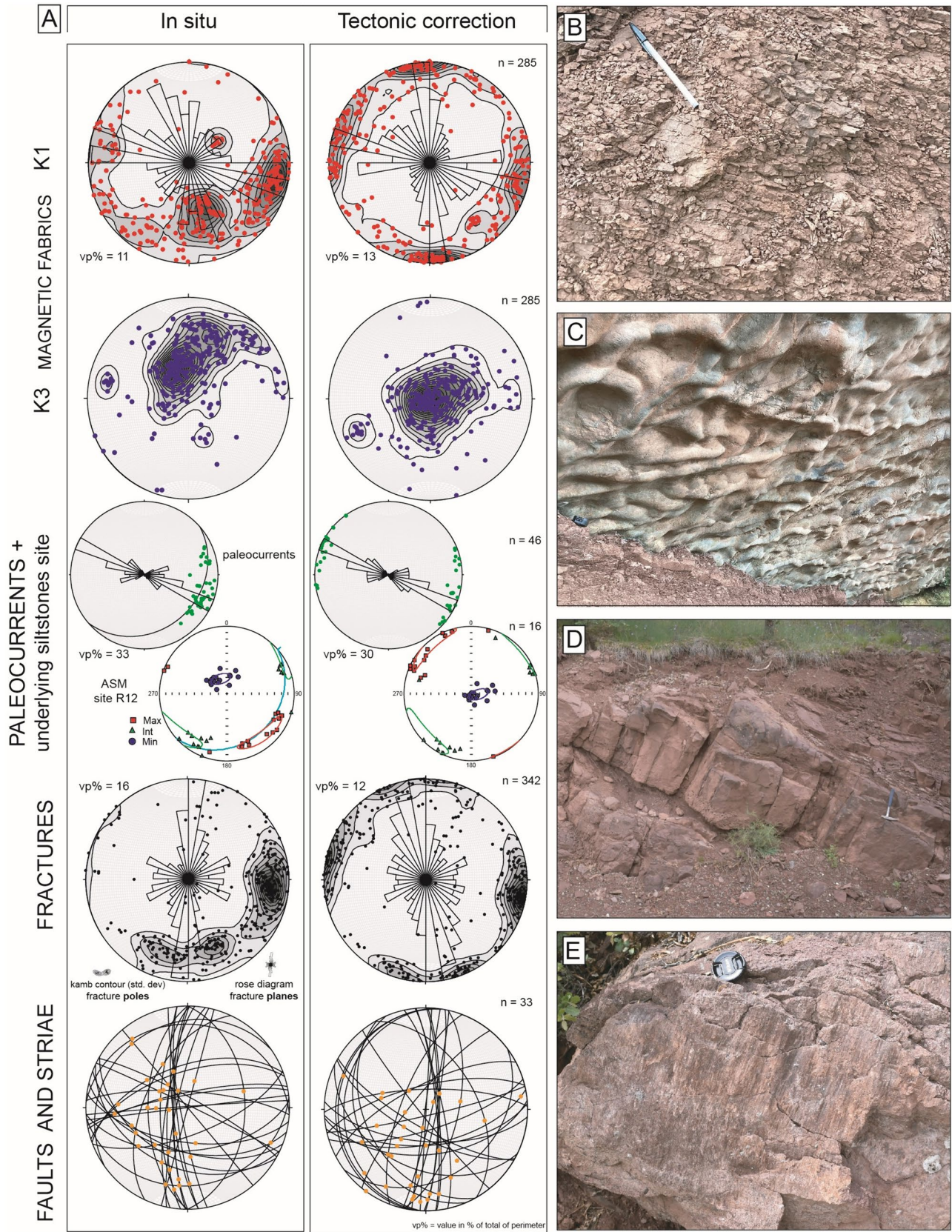
◄ **Fig. 7 A** Density diagrams (Kamb contours, 2% interval) of magnetic axes, data from individual specimens: K_1 (Kmax) and K_3 (Kmin). Paleocurrents, fractures and faults with striae collected in the studied rocks. All data are represented before (left) and after (right) tectonic correction. **B** Clasystones showing pervasive fractures. **C** Paleocurrents at the bottom of the Permian red bed unit. **D** E–W fractures in a red sandstones. **E** Fault plane with striae

large-scale faults. There are no differences in its orientation related to the stratigraphic position of the samples or the lithology of the sites. At outcrop scale, the K_3 mean axis is perpendicular to the bedding plane and the magnetic lineation is perpendicular (sites R7 and R9) or clearly oblique (R3 and R4) to the strikes of the two fracture sets (Fig. 9): N–S and WNW–ESE. Furthermore, K_3 approaches, at least in two cases (R4 and R9) the line of intersection between the main fracture sets (Fig. 10).

The paleocurrents have a majority WNW-ESE direction coincident with one of the K_1 clusters observed in the overall data set and in the rose diagram of mean directions (Fig. 11). At site level, site R12 sampled in the underlying claystones, presents a K_1 direction slightly oblique to the general trend. However, in a close-up view, a NW–SE direction, at a low angle to the mean paleocurrent direction (which rather approximates an E-W trend), can be distinguished.

5 Interpretation and discussion

5.1 Oriented irregular fragments methodology

The so-called "fragment methodology" in AMS studies has been previously and successfully applied in other areas where sampling by means of oriented blocks or core drilling is difficult or impossible (Gracia-Puzo et al., 2021). However, to our knowledge it had not been applied to oriented fragments. The sampling methodology applied in claystone sites solves the difficulties of using traditional sampling methods (manually oriented blocks or oriented cores taken with a drilling machine) due to the fragility of this lithology. Indeed, the dimension of fragments is always less than 1 cm in this work. In spite of the difficulty of orienting fragments of this size, because the plane of measurement is necessarily small, the results show α_{95} confidence angles similar to the sites analyzed by standard methods, in which both drilling machines and larger blocks were used. Magnetic fabrics orientation and their K_m, Pj and T parameters do not show anomalous values and allow ruling out additional uncertainty or errors. This methodology is successful and replicable in fine-grained lithologies such as siltstones and claystones that have undergone diagenesis processes leading to strong fragmentation and hardness of the fragments at the same time.

5.2 Correlation between magnetic fabrics and petrofabrics and/or structural elements

According to the rock magnetism characterization, the magnetic carriers of the susceptibility are a mixture of paramagnetic and ferromagnetic minerals. The paramagnetic fraction represents more than half of the total contribution to magnetic susceptibility in each analyzed site and can be attributed to the phyllosilicates commonly present in detrital rocks such as micas and clays (except in site R16 where the contribution is only ferromagnetic). The ferromagnetic fraction is represented by hematite (T_N 675ºC), occasionally magnetite (T_C 580ºC). The abrupt decay at T_C 120ºC in site R21 is possibly goethite.

A key point in the analysis of magnetic fabrics is to recognize whether their origin is primary, i.e. whether they were fully developed at early stages of sedimentation and reveal the strain pattern at the time of deposition (see, e.g. Larrasoaña et al., 2011; García-Lasanta et al., 2013 and references therein) or secondary (acquired during the tectonic history of the basin, e.g. including tectonic inversion). The studied sites in the Cadí Basin, regardless of their lithology, show a magnetic susceptibility ellipsoid typical for sedimentary fabrics: K_1 and K_2 axes are contained in the bedding plane and the K_3 axis is well-clustered and parallel to the bedding pole (Parés, 2015; Tarling & Hrouda, 1993). In spite of this, three sandstone sites show a prolate shape (considering the magnetic ellipsoid axis distribution or the negative T parameter values, R15, R17, R18, R19, R20, R21 and R22 sites). The fact that the K_2 and K_3 axes are arranged in a girdle and the K1 axis is well-clustered (prolate shape) points towards either (i) a transition from extensional/sedimentary fabrics to compressional fabrics or ii) mineralogical artifacts related to alteration and crystallization of other mineral phases, as occurring, for example, in the Triassic of the Argana basin in Morocco (Oliva-Urcia et al., 2016). Having a look at the literature, prolate magnetic fabrics in detrital sediments such as claystones, siltstones and sandstones are commonly related to tectonic deformation (tectonic fabrics). This prolate fabrics are often associated to particular mechanisms such as micro-folding, or S-C-like structures, among others (see Lüneburg et al., 1999 and references therein). However, in general they are interpreted as the result of a deformation mechanism that has affected a large area, what gives a pervasive magnetic lineation (K_1 axis) in a direction parallel to the trend of the macrostructure (e.g. folds in Bakhtari et al., 1998). It should be noted that, although prolate fabrics can be also related to more local tectonic settings, it is not always possible to recognize the local conditions that originated them when the exposure of the rock is not optimal (Szaniawski et al., 2020). The references to prolate fabrics are scarcer whenthey are associated with mineralogical changes and formation of new minerals due to mineralization fluids
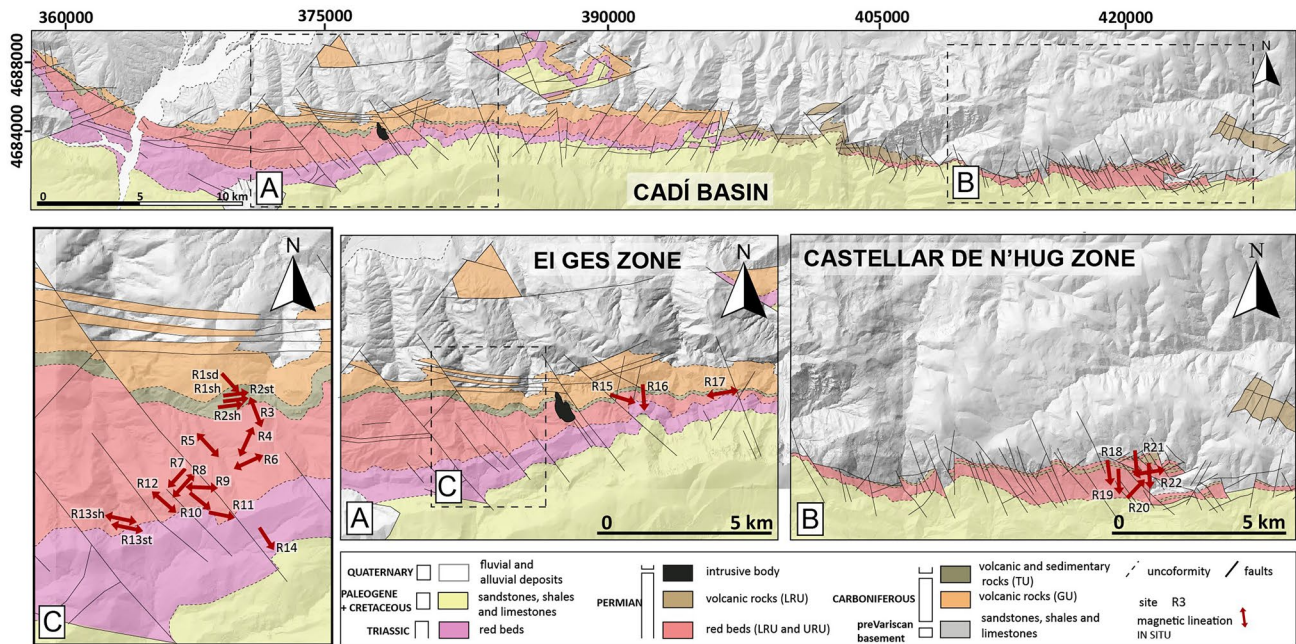
Fig. 8 In situ magnetic lineation (trend) plotted in the geological map (Gisbert, 1981). Rectangles indicate the location of the studied areas: **A** El Ges zone, **B** Castellar de n'Hug zone, and **C** Zoom in the El Ges zone. In the legend: GU—Grey Unit. TU—Transition Unit. LRU—Lower Red Unit. URU – Upper Red Unit
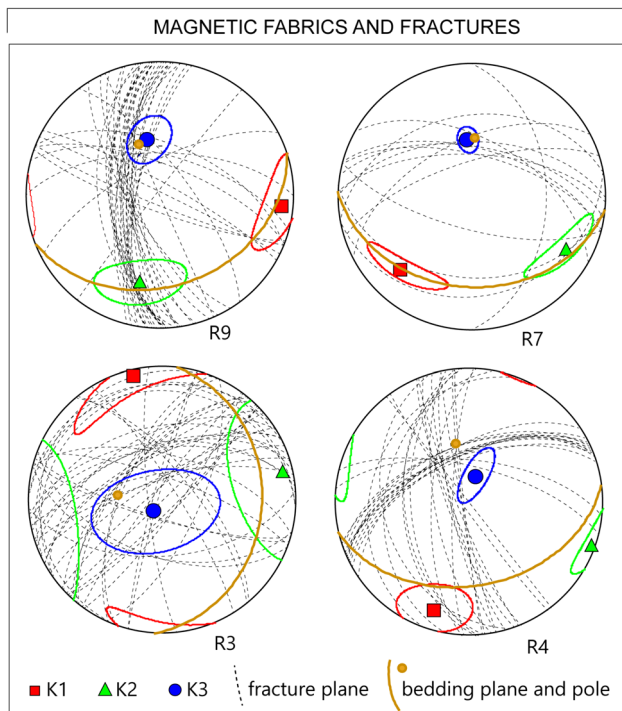

Fig. 9 Comparison between the magnetic ellipsoid (K_1, K_2 and K_3 axes) and structural data: fractures and bedding planes. Samples R3, R4, R7 and R9

(probably because only very detailed analysis under the FESEM can reveal them, Oliva-Urcia et al., 2016) but this origin cannot be discarded or ignored, either.

In the the present study in the Cadí Basin, most of the prolate fabrics do not show the expected (if a secondary origin related to compression is to be assumed) E–W trend (except for R15 and R17) of the main structure, the Cadí Range: a N-S and NNW–SSE directions are observed, instead. For that reason, mineralogical factors seem the most plausible explanation for these prolate magnetic fabrics.

Both K_1 and K_3 axes show better grouping after the tectonic correction considering the overall data. Most of the studied sites present a main common orientations for the magnetic lineation (K_1): WNW–ESE and close to N-S. This fact reveals that the primary stretching directions in red beds were constant along the time without remarkable changes. The interpretation of a stable stretching pattern is also reinforced by the parallelism between the paleocurrents directions measured in the base of conglomerates at the bottom of the Triassic sequence and the magnetic lineation in site R12 sampled in the underlying Permian red beds (LRU). This means that the water currents in the Cadí Basin flowed along a WNW-ESE direction, probably conditioned by the main and secondary faults (as it occurred during the Carboniferous for the volcanic and volcaniclastic rocks) in Triassic times.

In a more detailed view, the magnetic lineation orientation after tectonic correction is (i) oblique to the strike of
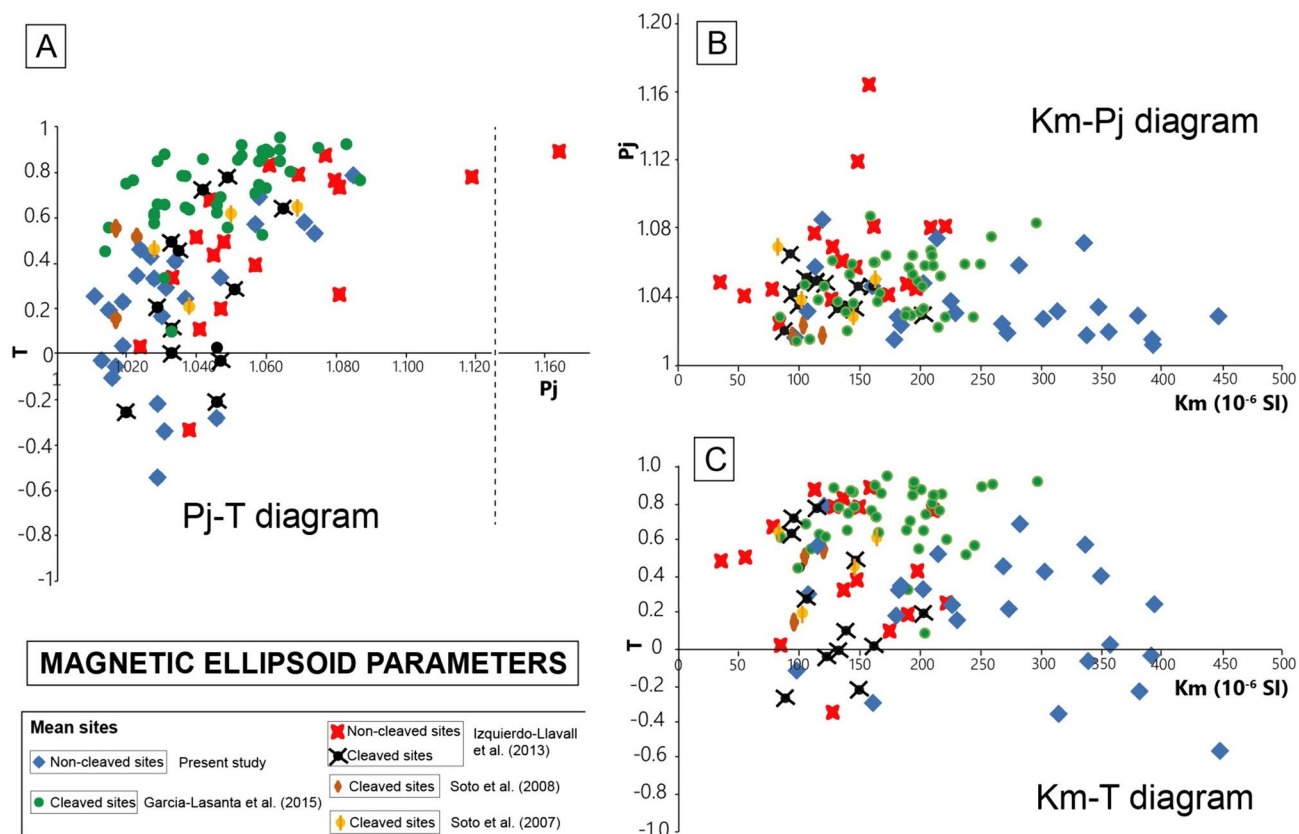
Fig. 10 Diagrams of the magnetic ellipsoid parameters and mean values at site level of the different studies performed in the Permian and Triassic rocks in the Iberian Peninsula: **A** Corrected anisot-ropy degree (Pj) versus shape parameter (T). **B** Corrected anisot-ropy degree (Pj) versus bulk magnetic susceptibility (Km). **C** Shape parameter (T) versus bulk magnetic susceptibility (Km)

the mapped, large-scale faults of the Cadí Basin (Gisbert et al., 2024), and (ii) perpendicular to the main faults with Pyrenean strike limiting the Triassic basins (Saura & Teixell, 2006) in five sites (R3, R5, R10, R12 and R20). We interpret in the latter case that the magnetic fabrics respond more to the local stretching tectonic context determined by the fault pattern that to the regional one represented by the N-S conjugate normal faults (Gisbert et al., 2024) controlling sedimentation in the Cadí Basin. This model is supported by the precipitation of hematite during diagenesis that also took advantage of the primary orientation of the platy minerals in fine-grained rocks, as observed in thin sections (Fig. 1D).

5.3 Magnetic lineation in the Cadí Basin and comparison with other Permian and Triassic basins in the Iberian plate.

There are several magnetic fabrics studies performed in Permian and Triassic basins in the northern Iberian Peninsula (García-Lasanta et al., 2015; Izquierdo-Llavall et al., 2013; Oliva-Urcia et al., 2006; Soto et al., 2007, 2008). For the comparison with the magnetic fabrics obtained in this

work, only results obtained in the Lower Triassic (Bunt-sandstein facies) and Permian were considered. In all cases, claystones, siltstones and fine/medium grained sandstones were selected to avoid as much as possible the influence of paleocurrents in the mineral arrangements. In these previ-ous studies, AMS results are described as tectonic fabrics because of their magnetic parameters and the relationship between the orientation of magnetic susceptibility axes and the regional structural markers such as faults, bedding, or cleavage planes.

In the Cabuérniga Basin, the Demanda-Cameros Massif and the Iberian Range, magnetic fabrics are interpreted as an early tectonic fabric related to the extensional syn-sedimentary context in Triassic times (García-Lasanta et al., 2015; Soto et al., 2007, 2008). However, in the Central Pyrenees (Oliva-Urcia et al., 2006 in the Bielsa sector and Izquierdo-Llavall et al., 2013 in the Nogueres Zone) magnetic fabrics are explained in terms of tectonic fabrics that show a tectonic overprint originated during the Eocene–Oligocene Pyrenean deformation (Alpine orog-eny). In all cases, the magnetic lineation orientation is explained in terms of stretching directions according to
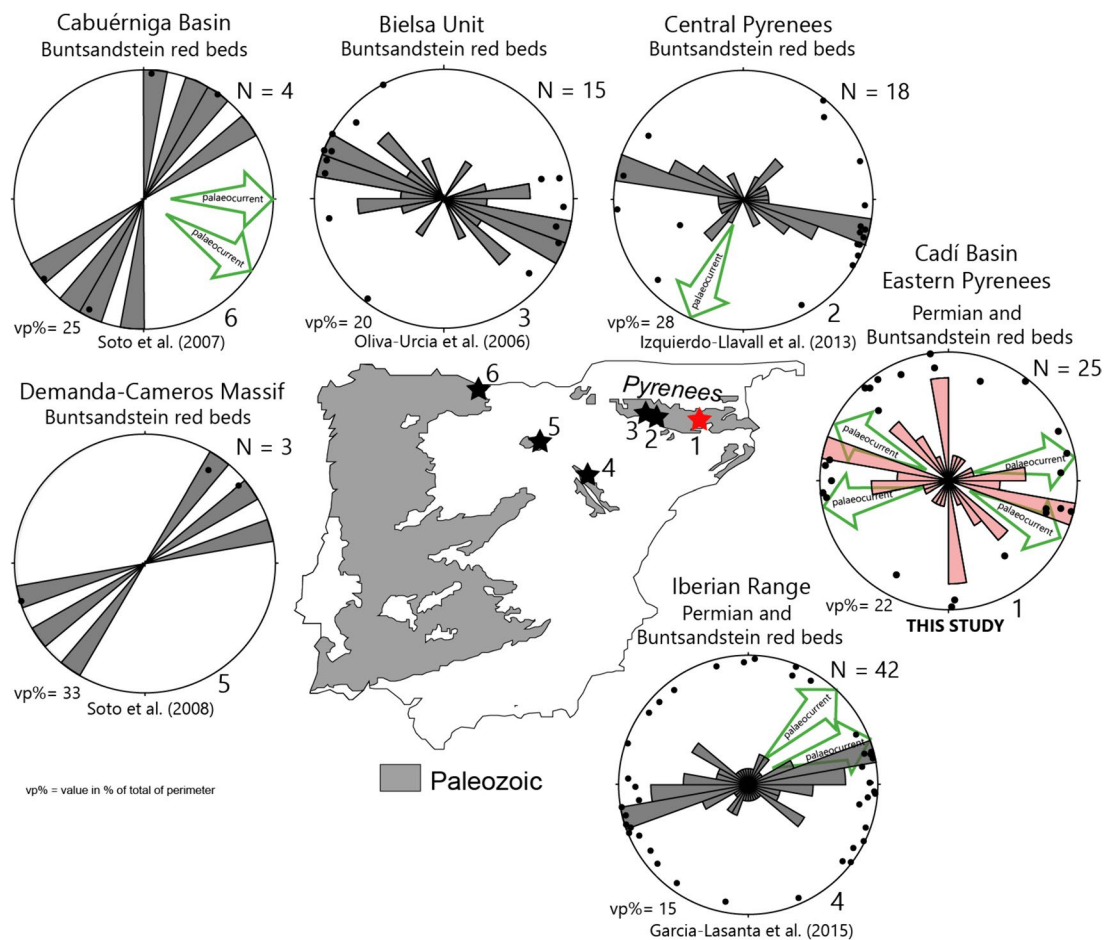
Fig. 11 Rose diagrams of the magnetic lineation (mean values at site level after tectonic correction) obtained in different studies performed in the Permian and Triassic rocks in the Iberian Peninsula. Green arrows: directions of paleocurrents measured in the studied rocks in the different zones

the orientation of faults (in the case of extensional origin) and cleavage (i.e. intersection between bedding and cleavage planes, when the magnetic fabric is compressional in origin), if present. The magnetic susceptibility parameters in red beds show that K_m values are usually under $300 \cdot 10^{-6}$ SI in all the studied basins except in the Cadí Basin, where it reaches anomalously higher values: in ten out of 25 sites it ranges between 301.9 and $446.4 \cdot 10^{-6}$ SI regardless of the lithology (Fig. 10). We interpret that these higher K_m values are related to magnetite content in the mineral assemblage, as the temperature-dependent magnetic susceptibility curves point out. However, the presence of magnetite has not been observed in the other basins or its presence has been considered negligible (see Izquierdo-Llavall et al., 2013, 2018; García-Lasanta et al., 2015). In the same way, the Pj and T parameters hardly show any correlation, what indicates that there is no influence of the magnetic mineralogy on the mineral arrangement. This fact allows us to consider all the studied sites for the general geodynamic interpretation.

The studies carried out in the Central Pyrenees (Izquierdo-Llavall et al., 2013; Oliva-Urcia et al., 2006) are the ones that present more similarities in terms of its structural location and the main orientation, N110E, of the magnetic lineation (K_1) with the present study. Nevertheless, the secondary K_1 cluster with a NNW-SSE to N-S direction recorded in the Cadí Basin is not present in the previously studied areas in the Pyrenees or in any of the other Permian basins in northern Iberia (Fig. 11), and can be related to a local stretching direction. This NNW-SSE magnetic lineation direction is found not only in the sedimentary red beds but also (although with a slightly NNE-SSW direction) in the volcanic and volcaniclastic rocks (Simón-Muzás et al., 2022). In this way, the E-W syn-sedimentary faults described in the Cadí Basin (Gisbert, 1981) probably acted since the Carboniferous during the deposit of the volcanic/volcaniclastic rocks and throughout the Permian until the beginning of the Triassic, thus conditioning the deposit (location, and orientation of depocenters) of all these sediments. On the other hand, the main faults mapped in the Cadí Basin

(Gisbert et al., 2024), that show NNW-SSE and SW-NE strikes are arranged N-S after the tectonic correction of the whole stratigraphic series (Fig. 12 B). The main K_1 cluster (WNW-ESE direction) is probably related with the stretching direction associated with this set of faults.

In the Cadí Basin, the absence of Alpine cleavage (Choukroune & Séguret, 1973) is in contrast with its occurrence in the Central Pyrenees (Izquierdo-Llavall et al., 2013) in rocks of the same age and lithology. This, and the fact that in most sites magnetic fabrics present a typical sedimentary arrangement, indicate an early stretching direction during the deposition of the LRU and URU. This tectonic scenario continues along the Triassic and is also in continuity with the stress regime prevailing during the sedimentation of the Late Carboniferous volcanic and volcaniclastic rocks (Simón-Muzás, et al., 2022). A similar interpretation can be applied in the Central Pyrenees, where the tectonic corrected magnetic lineation presents the same main orientation, and can be considered as an early stretching direction, originated during the deposition of sediments. The paleomagnetic data

of Late-Carboniferous-Permian series of the Cadí basin point to the absence of regional vertical-axis rotations during subsequent tectonic events (Simón-Muzás et al., 2023). The observed magnetic lineations did not rotate and their orientation can be interpreted straightforwardly. A paleogeographic reconstruction of the Central Cadí Basin based on the geological map and the stratigraphic panel (Gisbert et al., 2024) allows us to understand the fault activity in the studied area (Fig. 12B) from the Late Carboniferous to the Triassic.

Attending the large-scale tectonic scenario, the magnetic lineation orientations in the Permian and Triassic rocks from the northern Iberian Peninsula allow us to hypothesize about the regional trajectories of stretching directions (σ_3 stress axes) in the northern Iberian plate during that period, due to the activity of the North-Pyrenean fault zone (Fig. 12A). Stretching directions become parallel to the North-Pyrenean fault zone in areas located next to it (Central and Eastern Pyrenees), being therefore compatible with a secondary extension at the tip of the strike-slip fault system. This is consistent with the geodynamic scenario during Triassic
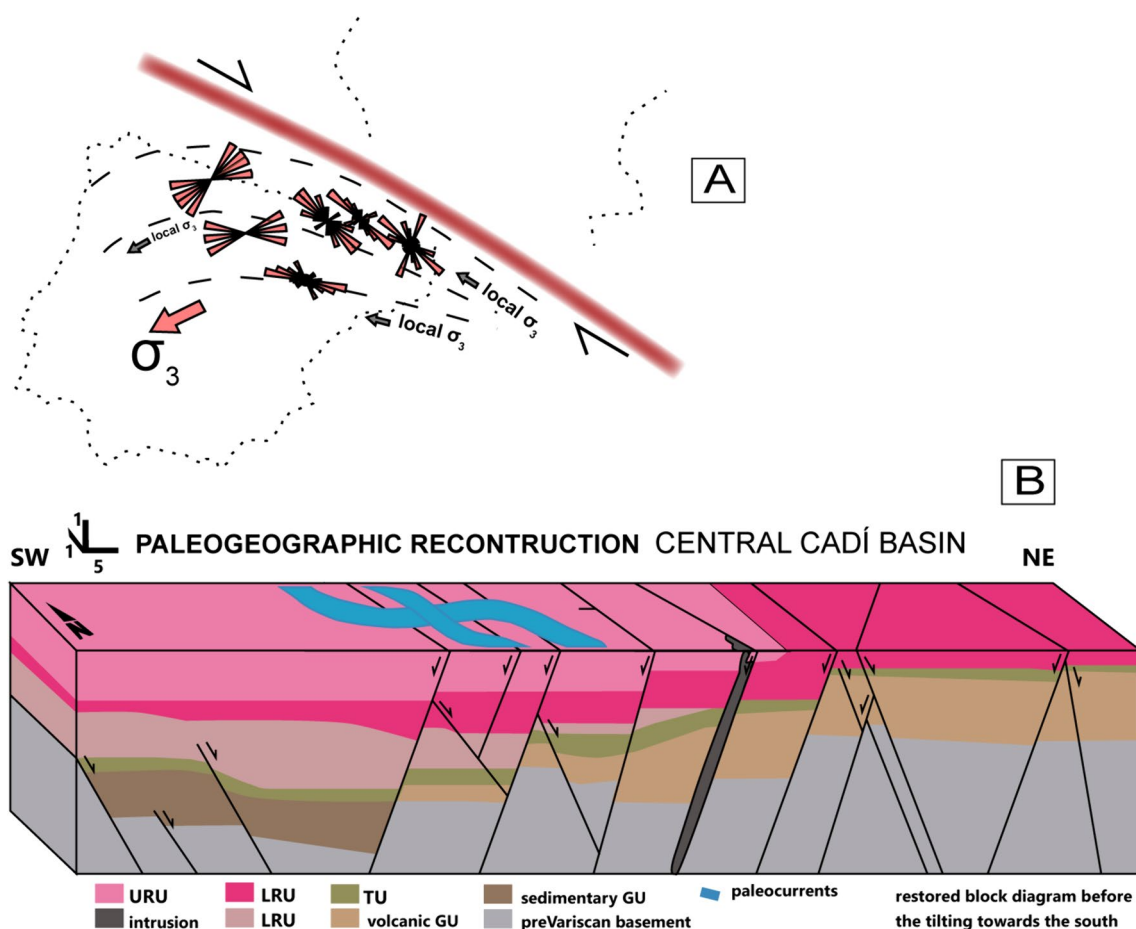
Fig. 12 **A** Reconstruction and interpretation of the main stretching directions in the Iberian plate during Permian and Triassic times; **B** Block diagram of the central area of the Cadí Basin (Castellar de

n'Hug is excluded) before the tilting of the stratigraphic sequence towards the south during the Pyrenean compression

times proposed by Soto et al. (2019), in which the North-Pyrenean fault zone would show a sinistral strike-slip motion.

Additionally, a local N-S direction is also recorded in the Cadí Basin but is only detected in some of the sandstones (prolate magnetic fabrics) and two siltstone sites. The fact that this direction is mainly recorded in sandstone sites can be related to mineralogical changes as it was pointed out in Sect. 5.2, even if this is not the most common mechanism. Despite this, if a tectonic origin is considered for this N-S direction it could be explained as the result of the deflection of the stretching trajectories. This could be related to the increasing distance to the zone of influence of the fault and the re-orientation of stress trajectories to become sub-perpendicular to the North-Pyrenean fault zone. In order to confirm one of the two hypotheses, it would be necessary to carry out a detailed magnetic sub-fabrics study in the red sandstones along the Permian–Triassic basins in the Pyrenees to observe if this N-S direction is recorded in other areas and if it is related or not to prolate magnetic fabrics. In any case, the proposed geodynamic context explains the magnetic lineation orientation after tectonic correction in the above-mentioned areas, including the Southern margin of the Iberian Massif (Dinarés-Turell & Parés, 1996) that shows a NE–SW direction.

6 Conclusions

The conclusions obtained in this study can be summarized as follows, from a local to a regional tectonic scenario:

– Red beds (claystones, siltstones and sandstones) reveal a primary magnetic fabric that recorded early stretching directions (in two nearly perpendicular directions, WNW-ESE and N-S) during the deposit of the rocks, linked to basin development.
– In the Cadí Basin, magnetic fabrics present a typical sedimentary fabric and indicate an early stretching direction during the deposition of the Upper Permian sediments (LRU and URU units) that continues along the Triassic, having started during the sedimentation of the Upper Carboniferous volcanic and volcanoclastic rocks.
– The stretching directions remained constant along time, without remarkable changes since the Late Carboniferous until the Triassic.
– The geodynamic scenario of the Iberian plate during the Late Permian–Triassic can be explained by the deflection of regional trajectories of σ_3 in the northern Iberian plate margin due to the strike-slip activity of the North-Pyrenean fault zone.
– The sampling methodology by means of oriented irregular fragments applied in siltstones and claystones has been proved as a useful way of obtaining samples in hard, however fragile lithologies. It is successful and replicable.

Declarations

References

Allmendinger, R. W., Cardozo, N., and Fisher, D. (2012). Structural geology algorithms: Vectors and tensors in structural geology: *Cambridge University Press*, *Cambridge*

Bakhtari, H. R., de Lamotte, D. F., Aubourg, C., Hassanzadeh, J. (1998). Magnetic fabrics of Tertiary sandstones from the Arc of Fars (Eastern Zagros, Iran). *Tectonophysics*, *284*(3-4), 299–316

Barnolas, A., Pujalte, V. (2004). La Cordillera Pirenaica. Geología de España, 233–241.

Bixel, F., (1984). Le Volcanisme Stéphano-Permien des Pyrénées. *Thèse d'Etat Université de Toulouse*, p. 639.

Chadima, M., Hrouda, F., (2012). Cureval 8.0: Thermomagnetic Curve Browser for Windows. Agico, Inc.

Chadima, M., Jelínek, V., (2019). Anisoft5.1.03: Anisotropy Data Browser for Windows. Agico, Inc.

Choukroune, P., & Séguret, M. (1973). *Carte structurale des Pyrénées*. Université des Sciences et Techniques du Languedoc.

Dinarés-Turell, J. D., & Parés, J. M. (1996). El Triásico de la Península Ibérica: Nuevos datos paleomagnéticos. *Cuadernos De Geología Ibérica, 20*, 367–384.

Felletti, F., Dall'Olio, E., & Muttoni, G. (2016). Determining flow directions in turbidites: An integrated sedimentological and magnetic fabric study of the Miocene Marnoso Arenacea Formation (northern Apennines, Italy). *Sedimentary Geology, 335*, 197–215.

García-Lasanta, C., Oliva-Urcia, B., Román-Berdiel, T., Casas, A. M., Gil-Peña, I., Sánchez-Moya, Y., Sopeña, A., Hirt, A. M., & Mattei, M. (2015). Evidence for the Permo-Triassic transtensional rifting in the Iberian Range (NE Spain) according to magnetic fabrics results. *Tectonophysics, 651*, 216–231.

García-Lasanta, C., Oliva-Urcia, B., Román-Berdiel, T., Casas, A. M., & Pérez-Lorente, F. (2013). Development of magnetic fabric in sedimentary rocks: Insights from early compactional structures. *Geophysical Journal International, 194*(1), 182–199.

Gisbert, J., (1981). Estudio geológico-petrológico del Estefaniense-Pérmico de la Sierra del Cadí (Pirineo de Lérida): Diagénesis y Sedimentología (Ph.D. thesis). University of Zaragoza

Gisbert, J., Simón-Muzás, A., Casas-Sainz, A. M., Soto, R. (2024). Geology of the Late Carboniferous, Permian and Early Triassic basins of the Eastern Pyrenees. *Journal of Maps*

Gracia-Puzo, F., Aubourg, C., Casas-Sainz, A. (2021). A fast way to estimate the clay fabric from shale fragments. Key example from a strained thrust footwall (Pyrenees). *Journal of Structural Geology*, 152, 104443.

Graham, J. W. (1954). Magnetic susceptibility anisotropy, an unexploited petrofabric element. *Geological Society of America Bulletin, 65*, 1257–1258.

Gretter, N., Ronchi, A., López-Gómez, J., Arche, A., De la Horra, R., Barrenechea, J., & Lago, M. (2015). The Late Palaeozoic-Early Mesozoic from the Catalan Pyrenees (Spain): 60 Myr of environmental evolution in the frame of the western peri-Tethyan palaeogeography. *Earth-Science Reviews, 150*, 679–708.

Hartevelt, J. J. A. (1970). Geology of the upper Segre and Valira valleys, central Pyrenees. *Andorra/spain. Leidse Geologische Mededelingen, 45*(1), 167–236.

Hrouda, F. (1994). A technique for the measurement of thermal changes of magnetic susceptibility of weakly magnetic rocks by the CS-2 apparatus and KLY-2 Kappabridge. *Geophysical Journal International, 118*, 604–612.

Izquierdo-Llavall, E., Casas Sainz, A. M., Oliva-Urcia, B., Villalaín, J. J., Pueyo, E., Scholger, R. (2018). Rotational kinematics of basement antiformal stacks: paleomagnetic study of the western Nogueras Zone (Central Pyrenees). *Tectonics*, *37*(10), 3456–3478).

Izquierdo-Llavall, E., Casas-Sainz, A., & Oliva-Urcia, B. (2013). Heterogeneous deformation recorded by magnetic fabrics in the Pyrenean Axial Zone. *Journal of Structural Geology, 57*, 97–113.

Jelinek, V., 1977. *The Statistical Theory of Measuring Anisotropy of Magnetic Susceptibility of Rocks and Its Application,* Brno, Geofyzika, 88pp.

Jelinek, V. (1981). Characterization of the magnetic fabric of rocks. *Tectonophysics, 79*, 63–70.

Khan, M. A. (1962). Anisotropy of magnetic susceptibility of some igneous and metamorphic rocks. *Journal of Geophysical Research, 67*, 2873–2885.

Knight, M. D., & Walker, G. P. (1988). Magma flow directions in dikes of the Koolau Complex, Oahu, determined from magnetic fabric studies. *J. Geophys. Res. Solid Earth, 93*(B5), 4301–4319.

Kodama, K. P., & Sun, W. W. (1992). Magnetic anisotropy as a correction for compaction-caused paleomagnetic inclination shallowing. *Geophysical Journal International, 111*, 465–469.

Larrasoaña, J. C., Gómez-Paccard, M., Giralt, S., & Roberts, A. P. (2011). Rapid locking of tectonic magnetic fabrics in weakly deformed mudrocks. *Tectonophysics, 507*(1–4), 16–25.

Larrasoaña, J. C., Pueyo, E. L., & Parés, J. M. (2004). An integrated AMS, structural, palaeo- and rock-magnetic study of the Eocene marine marls from the Jaca-Pamplona basin (Pyrenees, N Spain); new insights into the timing of magnetic fabric acquisition in weakly deformed mudrocks. Magnetic Fabric: Methods and Applications (Edited by: Martín-Hernández, F., Lüneburg, C. M., Aubourg, C. & Jackson, M.). *Geological Society of London Special Publication, 238*, 127–144.

Lowrie, W. (1990). Identification of ferromagnetic minerals in a rock by coercivity and unblocking temperature properties. *Geophysical Research Letters, 17*(2), 159–162.

Lüneburg, C. M., Lambert, S. A., Lebit, H. D., Hirt, A. M., Casey, M., Lowrie, W. (1999). Magnetic anisotropy, rock fabrics and finite strain in deformed sediments of SW Sardinia (Italy). *Tectonophysics, 307*(1–2), 51–74.

Martín-Hernández, F., Hirt, A. M. (2003). The anisotropy of magnetic susceptibility in biotite, muscovite and chlorite single crystals. *Tectonophysics, 367*(1–2), 13–28.

Muñoz, J. A. (1992). Evolution of a continental collision belt: ECORS-Pyrenees crustal balanced cross-section. In *Thrust tectonics* (pp. 235–246). Springer, Dordrecht

Muñoz, J. A. (2019). Alpine orogeny: Deformation and structure in the northern Iberian margin (Pyrenees sl). *The Geology of Iberia: A Geodynamic Approach*: Volume 3: The Alpine Cycle, 433–451.

Nye, J. F. (1957). *The Physical Properties of Crystals: Their Representation by Tensors and Matrices* (p. 333). Clarendon Press.

Oliva-Urcia, B., Pueyo E. L.; Casas, A. M., (2006). Fábricas en el Triásico de la lámina de Bielsa (Pirineo Axial): ¿Indicadoras de distinto grado de deformación? In: MAGIBER I: Paleomag-netismo en la Península Ibérica. Univ. de Burgos, ISBN: 84–96394–35–2, 103–114 pp.

Oliva-Urcia, B., Casas, A. M., Moussaid, B., Villalaín, J. J., El Ouardi, H., Soto, R., Torres-López, S., & Román-Berdiel, T. (2016). Tectonic fabrics vs. Mineralogical artifacts in AMS analysis: A case study of the Western Morocco extensional Triassic basins. *Journal of Geodynamics, 94*, 13–33.

Oliva-Urcia, B., Larrasoaña, J. C., Pueyo, E. L., Gil, A., Mata, P., Parés, J. M., & Pueyo, O. (2009). Disentangling magnetic subfabrics and their link to deformation processes in cleaved sedimentary rocks from the Internal Sierras (west central Pyrenees, Spain). *Journal of Structural Geology, 31*(2), 163–176.

Parés, J.M., Van der Pluijm, B.A., 2002. Phyllosilicate fabric characterization by Lowtemperature anisotropy of magnetic susceptibility (LT-AMS). Geophys. Res. Lett. 29 (24).

Parés, J. M. (2015). Sixty years of anisotropy of magnetic susceptibility in deformed sedimentary rocks. *Frontiers in Earth Science, 3*, 4.

Parés, J. M., van der Pluijm, B., & Dinares-Turell, J. (1999). Evolution of magnetic fabrics during incipient deformation of mudrocks (Pyrenees, northern Spain). *Tectonophysics, 307*, 1–14. https://doi.org/10.1016/S0040-1951(99)00115-8

Piper, J. D. A., Elliot, M. T., & Kneller, B. C. (1996). Anisotropy of magnetic susceptibility in a Palaeozoic flysch basin: The Windermere Supergroup, northern England. *Sedimentary Geology, 106*(3–4), 235–258.

Pocoví, A., Pueyo Anchuela, Ó., Pueyo, E. L., Casas-Sainz, A. M., Román Berdiel, M. T., Gil Imaz, A., Ramajo Cordero, J., Mochales, T., García Lasanta, C., Izquierdo, E., Parés, J. M., Sánchez, E., Soto Marín, R., Oliván, C., Rodríguez Pintó, A., Oliva-Urcia, B., Villalaín, J. J., (2014). Magnetic fabrics in the Central-Western Pyrenees: an overview. In: ASM in deformed rocks a tribute to Graham J. Borradaile. Edited by: Almqvist, B.; Henry, B.; Jackson, M.; Werner, T.; Lagroix, F. *Tectonophysics* 629, 303–318.

Porquet, M., Pueyo, E. L., Román-Berdiel, M. T., Olivier, P., Longares, L. A., Cuevas, J., Ramajo, J., Antolín, B., Aranguren, A., Auréjac, J. B., Bouchez, J. L., Casas, A. M., Denèle, Y., Gleizes, G., Hilario, A., Izquierdo-Llavall, E., Leblanc, D., Oliva-Urcia, B., Santana, V., … Vegas, N. (2017). Anisotropy of magnetic susceptibility of the Pyrenean granites. *Journal of Maps, 13*(2), 438–448.

Pueyo-Anchuela, Ó. Gil-Imaz, A., Pocoví-Juan, A. (2010). Significance of AMS in multilayer systems in fold-and-thrust belts. A case study from the Eocene turbidites in the southern Pyrenees (Spain). *Geological Journal*, 45(5-6), 544–561.

Riedel, H., (1993): Fracture Mechanisms, in: Materials Science and Technology, R.-W. Cahn, P. Haasen and E.J. Kramer, Eds., Vol. 6: Plastic Deformation and Fracture of Materials, H. Mughrabi, Vol.-Ed., Chap. 12, VCH-Verlag, Weinheim, pp. 565–633.

Saura, E., & Teixell, A. (2006). Inversion of small basins: Effects on structural variations at the leading edge of the Axial Zone antiformal stack (Southern Pyrenees, Spain). *Journal of Structural Geology, 28*(11), 1909–1920.

Simón-Muzás, A., Casas-Sainz, A. M., Soto, R., Pueyo, E. L., Beamud, E., Oliva-Urcia, B. (2023). Paleomagnetic study of Late-Carboniferous-Permian rocks from the Cadí Basin (Eastern Pyrenees): Tectonic implications. *Tectonophysics*, 230148.

Simón-Muzás, A., Casas-Sainz, A. M., Soto, R., Gisbert, J., Román-Berdiel, T., Oliva-Urcia, B., Pueyo, E. L., & Beamud, E. (2022). Axial longitudinal flow in volcanic materials of the Late Carboniferous-Permian Cadí basin (Southern Pyrenees) determined from anisotropy of magnetic susceptibility. *Journal of Volcanology and Geothermal Research, 421*, 107443.

Soto, R., Casas-Sainz, A. M., Oliva-Urcia, B., García-Lasanta, C., Izquierdo-Llavall, E., Moussaid, B., Kullberg, J. C., Román-Berdiel, T., et al. (2019). Triassic stretching directions in Iberia and North Africa inferred from magnetic fabrics. *Terra Nova, 2019*(31), 465–478.

Soto, R., Casas-Sainz, A. M., Villalaín, J. J., Gil-Imaz, A., Fernández-González, G., Del Río, P., Calvo, M., & Mochales, T. (2008). Characterizing the Mesozoic extension direction in the northern Iberian plate margin by anisotropy of magnetic susceptibility (AMS). *Journal of the Geological Society, 165*, 1007–1018.

Soto, R., Casas-Sainz, A. M., Villalaín, J. J., & Oliva-Urcia, B. (2007). Mesozoic extension in the Basque-Cantabrian basin (N Spain. Contributions from AMS and brittle mesostructures. *Tectonophysics, 445*, 373–394.

Soto, R., Larrasoaña, J. C., Arlegui, L. E., Beamud, E., Oliva-Urcia, B., & Simón, J. L. (2009). Reliability of magnetic fabric of weakly deformed mudrocks as a palaeostress indicator in compressive settings. *Journal of Structural Geology, 31*(5), 512–522.

Stachowska, A., Łoziński, M., Śmigielski, M., Wysocka, A., Jankowski, L., & Ziółkowski, P. (2020). Anisotropy of magnetic susceptibility as an indicator for palaeocurrent analysis in folded turbidites (Outer Western Carpathians, Poland). *Sedimentology, 67*(7), 3783–3808.

Szaniawski, R., Ludwiniak, M., Mazzoli, S., Szczygiel, J., Jankowski, L. (2020). Paleomagnetic and magnetic fabric data from Lower Triassic redbeds of the Central Western Carpathians: new constraints on the paleogeographic and tectonic evolution of the Carpathian region. *Journal of the Geological Society*. *177*(3), 509–522. https://doi.org/10.1144/jgs2018-232

Tarling, D., & Hrouda, F. (Eds.). (1993). *Magnetic anisotropy of rocks*. Springer.

Vergés, J., Fernàndez, M., Martínez, A. (2002). The Pyrenean orogen: pre-, syn-, and post-collisional evolution. In: Rosenbaum, G. and Lister, G. S. 2002. Reconstruction of the evolution of the Alpine-Himalayan Orogen. *Journal of the Virtual Explorer*, 8, 55 - 74.